THE JOURNAL OF BIOLOGICAL CHEMISTRY VOL. 292, NO. 4, pp. 1438–1448, January 27, 2017

Trp-Asp (WD) Repeat Domain 1 Is Essential for Mouse Peri-implantation Development and Regulates Cofilin Phosphorylation*

Received for publication, September 21, 2016, and in revised form, December 16, 2016 Published, JBC Papers in Press, December 19, 2016, DOI 10.1074/jbc.M116.759886

Yi Xiao[‡§], Haixia Ma[‡§], Ping Wan[¶], Dandan Qin[‡§], Xiaoxiao Wang[‡§], Xiaoxin Zhang[‡], Yunlong Xiang[‡], Wenbo Liu[‡], Jiong Chen[¶1], Zhaohong Yi[‖2], and Lei Li[‡§3]

From the [‡]State Key Laboratory of Stem Cell and Reproductive Biology, Institute of Zoology, Chinese Academy of Sciences, 100101 Beijing, the [§]Institute of Zoology, University of Chinese Academy of Sciences, Beijing 100049, the [¶]State Key Laboratory of Pharmaceutical Biotechnology and MOE Key Laboratory of Model Animals for Disease Study, Model Animal Research Center, Nanjing University, Nanjing 210061, and the [‖]Key Laboratory of Urban Agriculture (North) of Ministry of Agriculture, College of Biological Science and Engineering, Beijing University of Agriculture, Beijing 102206, China

Edited by Xiao-Fan Wang

Trp-Asp (WD) repeat domain 1 (WDR1) is a highly conserved actin-binding protein across all eukaryotes and is involved in numerous actin-based processes by accelerating Cofilin severing actin filament. However, the function and the mechanism of WDR1 in mammalian early development are still largely unclear. We now report that WDR1 is essential for mouse peri-implantation development and regulates Cofilin phosphorylation in mouse cells. The disruption of maternal WDR1 does not obviously affect ovulation and female fertility. However, depletion of zygotic WDR1 results in embryonic lethality at the peri-implantation stage. In WDR1 knock-out cells, we found that WDR1 regulates Cofilin phosphorylation. Interestingly, WDR1 is overdosed to regulate Cofilin phosphorylation in mouse cells. Furthermore, we showed that WDR1 interacts with Lim domain kinase 1 (LIMK1), a well known phosphorylation kinase of Cofilin. Altogether, our results provide new insights into the role and mechanism of WDR1 in physiological conditions.

The actin cytoskeleton is a highly dynamic structure that regulates cell motility, adhesion, division, and growth and has a fundamental function in embryonic development (1–3). In physiological conditions, actin filaments are continually assembled and disassembled in response to varied cellular activities (4, 5). The dynamics of F-actin is well orchestrated by a large number of actin-binding proteins (5, 6). Actin-depolymerizing factor Cofilin plays critical roles in the modulation of actin cytoskeleton dynamics (7). *In vitro*, Cofilin severs actin filament at low concentrations, whereas it fully decorates actin filaments and suppresses the severing activity at high concentrations (8, 9). In addition, Cofilin severing F-actin is not explained well for how the filaments of actin cytoskeleton can be rapidly disassembled in physiological conditions (4). Thus, the function of Cofilin in actin dynamics depends not only on its relative concentration to actin, but also on other regulatory proteins *in vivo*. Dysfunction of these regulating proteins results in aberrant actin cytoskeleton in various cellular and developmental processes (10–12).

Cofilin directly binds with actin to function as a regulator of the actin dynamics (13). However, the phosphorylation of Cofilin at Ser-3 blocks its binding site to actin (14, 15). Thus, the activity of Cofilin is controlled by phosphorylation and dephosphorylation processes, which are regulated by cascade reactions of several protein kinases and phosphatases. Lim domain kinases (LIMKs)[4] and testis-specific protein kinases (TESKs) are responsible for the phosphorylation of Cofilin, whereas slingshot (SSH) family protein phosphatases and pyridoxal phosphatase (PDXP) catalyze the dephosphorylation reaction (16–20). These kinases and phosphatases are also regulated by their phosphorylation or localization in cytoplasm to maintain the level of Cofilin phosphorylation in response to extracellular stimuli (21–23).

The activity of Cofilin on actin disassembly is greatly accelerated by other actin-binding proteins (24, 25). WDR1 (WD40 domain repeat 1, also known as actin interaction protein 1), is conserved and was originally identified as an actin-binding protein by a yeast two-hybrid screen (26). WDR1 is involved in actin dynamics by promoting the actin disassembly activity of Cofilin. Mutations in WDR1 result in abnormal cytoskeletal behavior in many organisms (27–29). A Gene-trap vector inserted *Wdr1* intron 2 disrupts its expression completely and results in embryonic lethality before E10.5 (embryonic day

* This work was supported by National Natural Science Foundation of China Grants 31590832 and 31471353 and Strategic Priority Research Program of the Chinese Academy of Sciences Grant XDA01010103. The authors declare that they have no conflicts of interest with the contents of this article.

[1] To whom correspondence may be addressed. Tel.: 86-25-58641507; Fax: 86-25-58641507; E-mail: chenjiong@nju.edu.cn.
[2] To whom correspondence may be addressed. Tel.: 86-10-80799114; Fax: 86-10-80799114; E-mail: yizhaoh2009@163.com.
[3] To whom correspondence may be addressed. Tel.: 86-10-64807465; Fax: 86-10-64807865; E-mail: lil@ioz.ac.cn.

[4] The abbreviations used are: LIMK, Lim domain kinase; WDR1, Trp-Asp (WD) repeat domain 1; LIMK1, Lim domain kinase 1; TESKs, testis-specific protein kinases; SSH, slingshot; PDXP, pyridoxal phosphatase; GV, germinal vesicle; MII, metaphase II; EB, embryoid body; IP, immunoprecipitation; oKO, oocyte-specific knock-out; MEF, mouse embryonic fibroblast; PI, propidium iodide; iKO, inducible knock-out; LIF, leukemia inhibitory factor; EGFP, enhanced green fluorescent protein; EdU, 5-ethynyldeoxyuridine; CTL, control.

10.5) in mice, whereas a hypomorphic insertion mutation in this gene leads to autoinflammatory disease because of the impairment of cytoskeletal response in neutrophils and thrombopoiesis (27). WDR1-mediated actin disassembly is also required for spermatogenesis and myocardial growth in mice (30, 31). In humans, the aberrant expressions of WDR1 have been shown to be connected to several diseases, including gout, pancreatitis, and primary glioblastoma (32–34). Although WDR1 is critical for numerous physiological conditions, how it acts in early embryonic development remains largely unclear.

In our study, we demonstrated that zygotic, but not maternal, expression of WDR1 is important for mouse early embryonic development. We showed that WDR1 is essential for mouse peri-implantation development. Most interestingly, we found that WDR1 regulates the level of Cofilin phosphorylation through LIMK, a novel mechanism of WDR1 involved in Cofilin activity.

Results

Zygotic, Not Maternal, WDR1 Is Required for Mouse Development—To investigate the function of *Wdr1* in oocyte maturation and pre-implantation embryogenesis, we first examined the expression of *Wdr1* in mouse oocytes and pre-implantation embryos by quantitative RT-PCR and Western blotting analysis. Our results showed that *Wdr1* mRNA was highly expressed in mouse germinal vesicle (GV) oocytes, decreased in metaphase II (MII) oocytes, 1-cell, 2-cell, and morula stage embryos, and then sharply increased in blastocyst stage embryos (Fig. 1*A*). By comparison, Western blotting analysis showed that WDR1 protein was comparatively highly expressed in GV oocytes, decreased in MII oocytes, increased in 1-cell and 2-cell embryos, and decreased in morula and blastocyst stage embryos again (Fig. 1*B*).

We generated *Wdr1* oocyte-specific knock-out mice by mating $Wdr1^{f/f}$ mice with *Zp3-cre* transgenic mice to study the role of WDR1 in female fertility. The mRNA and protein of *Wdr1* were dramatically decreased in the GV oocytes from $Wdr1^{f/f}$; *Zp3-cre* (oocyte-specific knock-out, oKO) females as noted by quantitative RT-PCR and Western blotting analysis (Fig. 1, *C* and *D*). However, $Wdr1^{f/f}$; *Zp3-cre* females delivered comparable offspring compared with the controls ($Wdr1^{f/f}$ and $Wdr1^{f/+}$; *Zp3-cre* females) after mating with $Wdr1^{f/f}$ males (Fig. 1*E*). These data demonstrated that maternal WDR1 is not required for $Wdr1^{f/f}$; *Zp3-cre* female fertility.

We also mated $Wdr1^{f/f}$; *Zp3-cre* females with $Wdr1^{f/-}$ males. The litter size was decreased to about 50% (Fig. 1*E*), indicating *Wdr1* KO embryos was lost during embryonic development, consistent with a previous report in which severe loss function of WDR1 resulted in embryonic lethality before E10.5 (27). Thus, these results suggested that zygotic, but not maternal, expression of *Wdr1* is required for mouse development.

WDR1 Is Essential for Mouse Peri-implantation Development—To examine the causes and time point of *Wdr1* KO embryo lethality, $Wdr1^{f/f}$; *Zp3-cre* and $Wdr1^{f/f}$ female mice mated with $Wdr1^{f/-}$ male mice and the deciduas were analyzed at E5.5. Our results showed that the number of deciduas per litter was 7–10 in both groups and were not obviously different

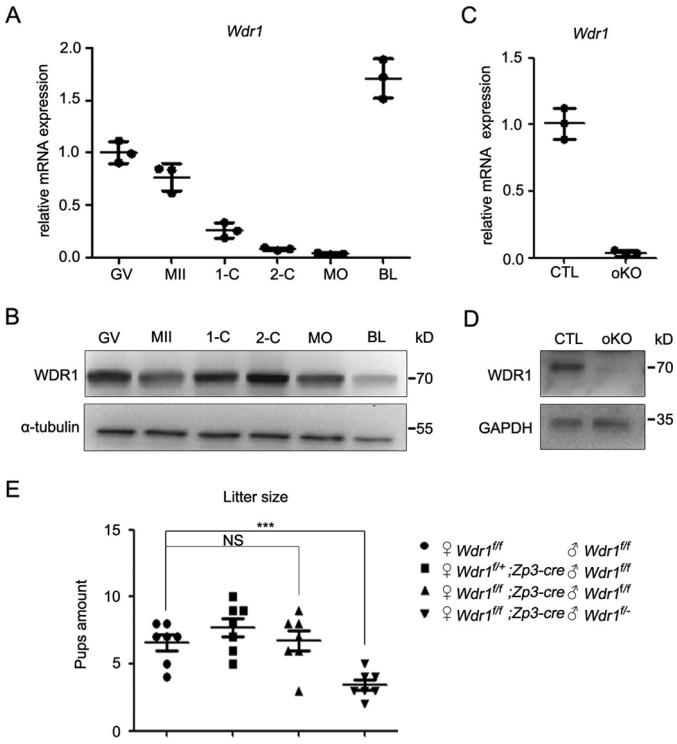

FIGURE 1. **Maternal knock-out of *Wdr1*.** *A, Wdr1* transcripts were detected in 50 GV oocytes, MII oocytes, zygotes (*1-C*), two-cell (*2-C*), morula (*MO*), and blastocyst (*BL*) stage embryos by quantitative RT-PCR. RNA expression in GV oocytes was set as 1. Data are represented as mean ± S.D. from three independent experiments. *B*, expression of WDR1 protein in oocytes and preimplantation embryos ($n = 50$) were analyzed by Western blotting analysis with α-tubulin as a loading control. *C, Wdr1* transcription was detected in 50 control or knock-out GV oocytes by real-time RT-PCR. RNA expression in control GV oocytes was set as 1. *Error bars* represent S.D. *D,* WDR1 protein was detected in 20 control or knock-out GV oocytes using GAPDH as a loading control. *E,* litter sizes of $Wdr1^{f/f}$, $Wdr1^{f/+}$, and $Wdr1^{f/f}$; *Zp3-cre* females after mating with $Wdr1^{f/f}$ males or $Wdr1^{f/f}$; *Zp3-cre* females after mating with $Wdr1^{f/-}$ males are presented as mean ± S.D. All litter sizes for each genotype were obtained from at least 3 females. ***, $p < 0.001$; *NS*, not significant.

from each other (Fig. 2*A*). However, after sectioning and H&E staining of these deciduas, 53% of the deciduas from $Wdr1^{f/f}$; *Zp3-cre* females had normal embryos (Fig. 2*B* (*a*)), and 47% had no embryos (Fig. 2*B* (*b*)), whereas the percentage of empty deciduas from $Wdr1^{f/f}$ females (control) was only 3% (Fig. 2*B*, *right panel*). These data indicated that the blastocysts lacking WDR1 were able to implant and induce the decidualization, but were absorbed at E5.5, suggesting that WDR1 is essential for mouse peri-implantation development.

To further investigate *Wdr1* KO embryonic development, blastocysts were obtained from the uteruses of the $Wdr1^{f/f}$; *Zp3-cre* females after mating with $Wdr1^{f/-}$ males at E3.5 and cultured *in vitro*. KO and control blastocysts could not be distinguished at E3.5 (Fig. 2*C*). All blastocysts grew, hatched, and adhered to the dish during the first 2 days of culturing. However, 55% (11 of 20) of embryos grew obviously smaller at the third day. No EdU incorporation was detected in the smaller embryos (Fig. 2*D*). We then examined the genotypes of these embryos by PCR with specific primers and found that the genotype of 81% (9 of 11) of the smaller embryos were $Wdr1^{-/-}$ (Fig. 2*E*). These data suggest loss of WDR1 has no obvious effect

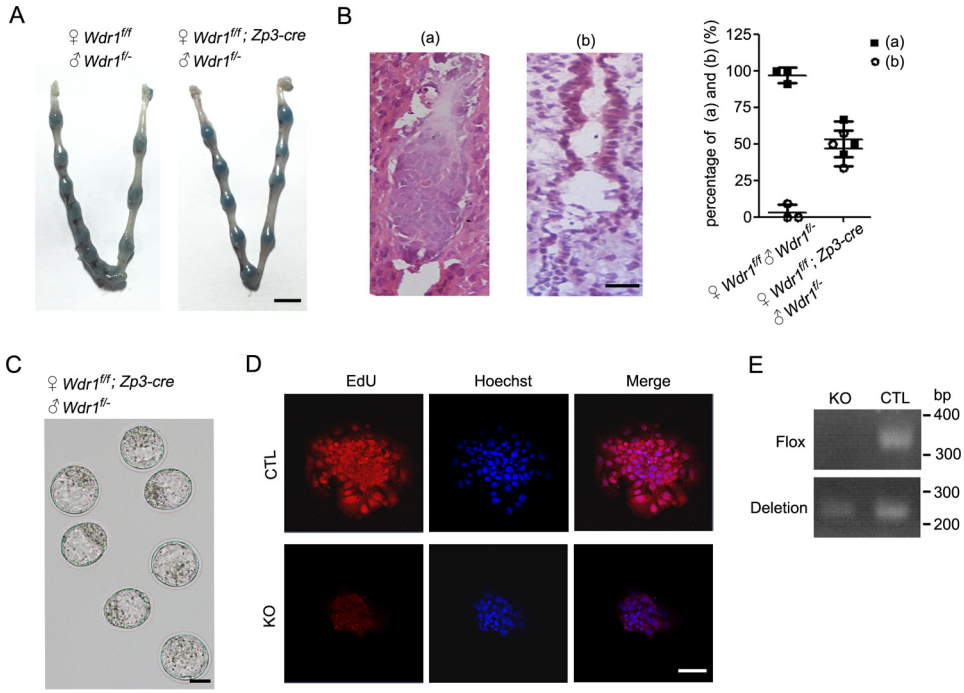

FIGURE 2. ***Wdr1* KO embryos in peri-implantation development.** *A,* after mating with $Wdr1^{f/-}$ males, oocyte specific knock-out females were injected with Chicago blue. Then, the uteruses were picked up at E5.5 and imaged by differential interference contrast. *Scale bar*, 5 mm. *B,* deciduas with embryos from *A* were frozen and sectioned (8 μm). The sections were stained by H&E and imaged. Two types such as (*a*) and (*b*) were observed. The percentage of the two types was counted from three pregnant females. Statistical results are represented as mean ± S.D. *Scale bar*, 50 μm. *C,* oocyte-specific *Wdr1* KO females were mated with $Wdr1^{f/-}$ males. At E3.5, blastocysts were flushed from the uterus and imaged by differential interference contrast. *Scale bar*, 40 μm. *D,* blastocysts obtained from *C* were cultured *in vitro* for 3 days and treated with EdU for 2 h before being fixed. The outgrowth was stained for EdU (*red*) according to the protocol provided by the manufacturer. Nuclear DNA was stained by Hoechst 33342 (*blue*). *Scale bar*, 200 μm. *E*, $Wdr1^{f/-}$ (control, *CTL*) and $Wdr1^{-/-}$ (knock-out, *KO*) embryos were genotyped with specific primers.

on blastocyst development, but cause the arrested development after adherence *in vitro*.

Wdr1 Knock-out Decreases Cofilin Phosphorylation in Mouse ES Cells—To investigate WDR1 functions in early embryos, we established ES cell lines from $Wdr1^{f/-}$ (control, CTL) and $Wdr1^{-/-}$ (knock-out, KO) blastocysts from $Wdr1^{f/f}$; *Zp3-cre* females after mating with $Wdr1^{f/-}$ males. The *Wdr1* mRNA and protein deletion were examined by real-time RT-PCR and Western blotting analysis in these ES cell lines (Fig. 3, *A* and *B*). *Wdr1* KO ES cells could be normally maintained in a 2i/leukemia inhibitory factor (LIF) medium and form typical clones (Fig. 3*D*). The expression of pluripotent markers such as NANOG, OCT4, and SOX2, and the cells proliferation were comparable in CTL and KO ES (Fig. 3, *B* and *C*).

To investigate their differentiation potentials, CTL and KO ES cells were labeled with EGFP and injected into normal blastocysts. These blastocysts were cultured for 3 days in an *in vitro* system of growing whole embryos. Our results showed that both CTL and KO ES cells incorporated into the cultured embryos detected by EGFP (Fig. 3*D*). The defect of *Wdr1* disruption on differentiation was further examined by embryoid bodies (EB) formation system, a model of ESC differentiation into germ layer lineages. Compared with their expressions at day 0 (d0), germ layer makers (*Sox17*, endoderm; *T*, mesoderm; *Pax6*, ectoderm) were comparably up-regulated in both CTL and KO EB at day 3 (d3) (Fig. 3*E*). These results indicate that WDR1 depletion may not affect the ES cells potential of differentiation.

Previous reports showed that WDR1 partial dysfunction (decreased to 20%) affected actin structure and depolarized Cofilin localization in migrating cells (27). Then, we examined F-actin and Cofilin in *Wdr1* KO ES cells by immunofluorescence. F-actin (*red*) was concentrated in the membrane in both knock-out ES cells and controls (Fig. 3*F*). The detailed actin structure could not be observed clearly in these cells. Surprisingly, different from WDR1 dysfunction in migrating cells (27), Cofilin was more concentrated to the membrane and co-located with actin filaments in $Wdr1^{-/-}$ ES cells, whereas it was more diffused in control (Fig. 3*F*). We also investigated phosphorylated Cofilin (P-Cofilin) by Western blotting analysis. Our results showed that the P-Cofilin level was much lower in $Wdr1^{-/-}$ ES cells than that in control (Fig. 3*G*). Then, we separated G-actin and F-actin from KO and control ES cells (35). Distinct from a previous report in *Wdr1* knockdown cells (36), F-actin level was not obviously increased in *Wdr1* KO ES cells as compared with the control (Fig. 3*H*). Altogether, *Wdr1* KO has no obvious impact on ES pluripotency and growth, but results in dramatically decreased P-Cofilin in these cells.

WDR1 Regulates the Phosphorylation of Cofilin and Controls F-actin in Mouse Embryonic Fibroblast (MEF) Cells—Interestingly, WDR1 expression is much higher in MEF cells than that in ES cells (Fig. 4*A*). To further investigate the effects of WDR1 on actin cytoskeleton, knock-out MEF cell lines were established by a tamoxifen induction system. $Wdr1^{f/-}$; $Cre\text{-}ER^{TM}$ fetuses were used to establish inducible knock-out (iKO) MEF

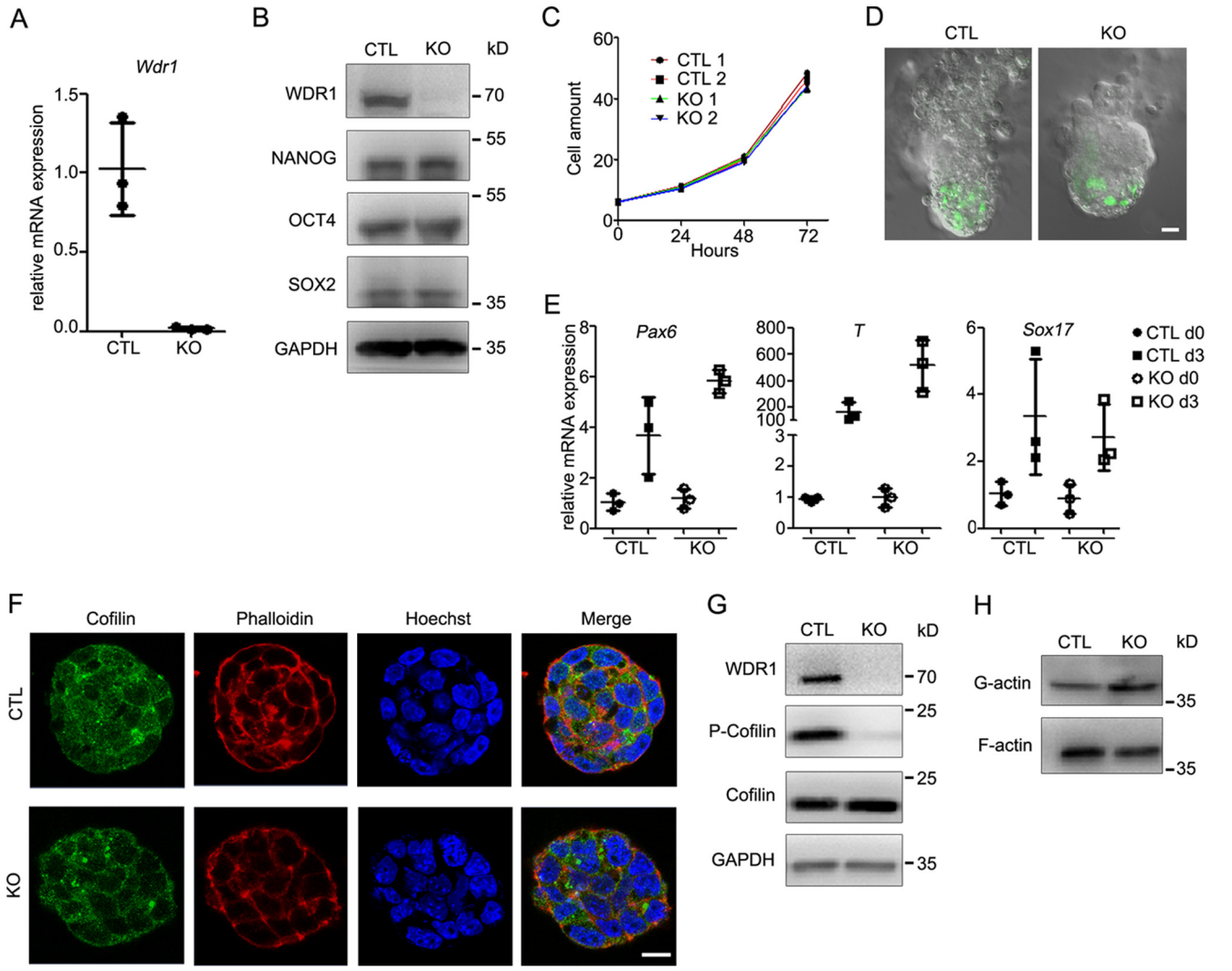

FIGURE 3. **Characterization of *Wdr1* KO ES cells.** *A,* total RNA samples from $Wdr1^{f/-}$ (control, *CTL*) and $Wdr1^{-/-}$ (knock-out, *KO*) ES were subjected to real-time RT-PCR to examine *Wdr1* transcription. *Gapdh* mRNA was used as a control. *B,* WDR1 and pluripotential markers NANOG, OCT4, and SOX2 were analyzed by Western blotting in CTL and KO ES cell lines, with GAPDH as a loading control. *C,* two KO and two CTL ES cell lines were cultured in a 12-well plate and the cells were counted every 24 h. Three wells for each cell line were examined at each time point. *D,* CTL and KO ES cells were labeled with EGFP and injected into normal blastocysts. After culturing 3 days, the embryos were examined by microscopy. *Scale bar*, 20 μm. *E, Pax6*, *T*, and *Sox17* transcription were examined by real-time RT-PCR in CTL and KO ES (*d0*) and 3 days EB (*d3*). *Gapdh* mRNA was used as a control. *F,* both CTL and *Wdr1* KO ES cells were fixed and incubated with a primary antibody to Cofilin. Then, these cells were incubated with FITC-tagged second antibody (Cofilin, *green*), Alexa Fluor® 546 Phalloidin (F-actin, *red*), and Hoechst 33342 (DNA, *blue*), and imaged. *Scale bar*, 20 μm. *G,* P-Cofilin and total Cofilin were detected by immunoblotting in CTL and *Wdr1* KO ES cells. GAPDH was used as a loading control. *H,* G-actin and F-actin were separated in control and *Wdr1* KO ES cell lines and probed with mouse anti-actin antibody.

lines, using $Wdr1^{+/-}$; $Cre\text{-}ER^{TM}$ MEF cells as the control (CTL). After 72 h treatment with tamoxifen, *Wdr1* mRNA and protein were decreased to 0.3 ± 0.018% and 4.5 ± 0.2%, respectively, compared with control (CTL) (Fig. 4, *B* and *C*). Actin plaques were observed in *Wdr1* iKO MEF cells, whereas the clear linear F-actin structure was shown in the control (Fig. 4*D*). However, we did not detect a significant increase in the overall F-actin level in *Wdr1* iKO MEF cells (Fig. 4*E*). P-Cofilin was observed to be dramatically decreased in *Wdr1* iKO MEF cells (Fig. 4*F*). We also examined the cell cycle by flow cytometry. Our results showed that control MEF cells had complete G_1, S, and G_2 cell stages, whereas *Wdr1* iKO MEF cells lost S stage and expanded G2 stage (Fig. 4*G*). These data suggested that the WDR1 loss affected MEF cell proliferation. Altogether, our results indicate that WDR1 regulates the formation of special actin plaques, the proliferation, and Cofilin phosphorylation in MEF cells.

WDR1 Regulates Phosphorylation of Cofilin in a Dose-independent Manner—The dramatically decreased P-Cofilin in *Wdr1* KO cells was inconsistent with a previous report for *Wdr1* knockdown cells (36), suggesting WDR1 might be overdosed in cells to regulate Cofilin phosphorylation. To test this hypothesis, we used the tamoxifen induction system to gradually reduce WDR1 content and examined the level of P-Cofilin during this process. WDR1, P-Cofilin, and Cofilin were detected in $Wdr1^{f/-}$; $Cre\text{-}ER^{TM}$ and control MEF cells after 0, 24, 48, and 72 h tamoxifen treatments. In $Wdr1^{f/-}$; $Cre\text{-}ER^{TM}$ MEF cells, WDR1 protein gradually reduced at the time course manner and almost failed to be detected at 72 h (Fig. 5*A*). Although the protein levels of WDR1 were obviously decreased at 24 and 48 h, P-Cofilin was comparable with the control at these time points. The decreased P-Cofilin was only clearly observed at 72 h after tamoxifen treatment (Fig. 5*A*). Consis-

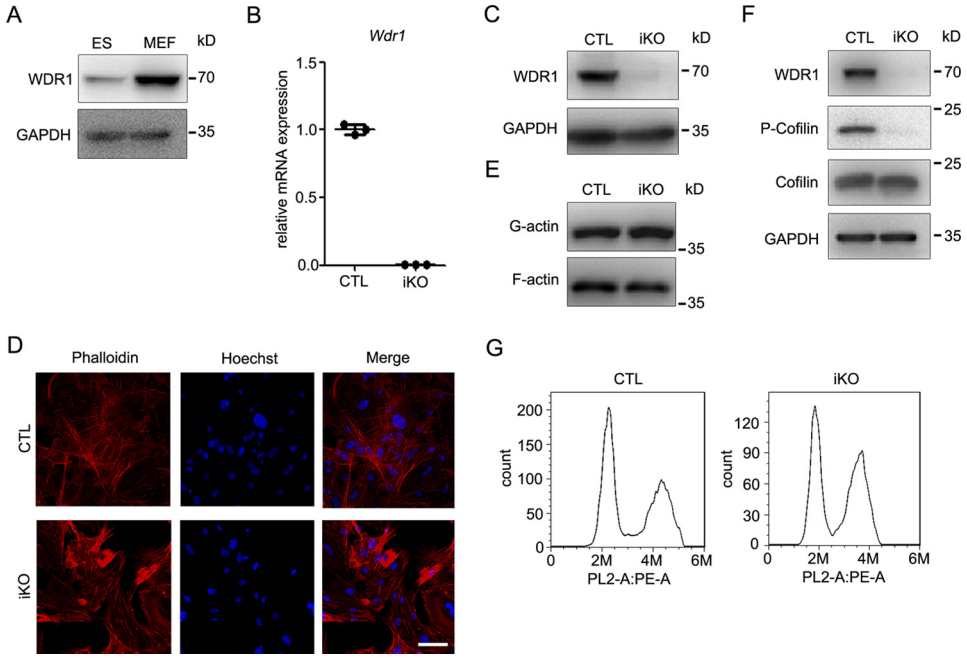

FIGURE 4. **Characterization of *Wdr1* mutant MEF cells.** *A,* WDR1 was analyzed by Western blotting in ES and MEF cells, with GAPDH as a loading control. *B*, *Wdr1* mRNA was detected by real-time RT-PCR in *Wdr1*$^{+/-}$; *Cre-ER*^{TM} (control, *CTL*) and *Wdr1*$^{f/-}$; *Cre-ER*^{TM} (*iKO*) MEF cells after being treated with tamoxifen for 72 h. *C*, immunoblot analyzed CTL and iKO MEF cells using WDR1 and GAPDH (loading control) antibodies. *D,* CTL and iKO MEF cells were stained by Alexa Fluor® 546 Phalloidin (F-actin, *red*) and Hoechst 33342 (DNA, *blue*), and imaged. *Scale bar*, 80 μm. *E*, G-actin and F-actin in CTL and iKO MEF cells were separated and probed by Western blotting with actin antibody. *F,* P-Cofilin, total-Cofilin, and WDR1 were detected in CTL and iKO MEF cells by Western blotting, using GAPDH as a loading control. *G*, after being treated with tamoxifen for 72 h, CTL and iKO MEF cells were digested, stained with PI, and examined by flow cytometry.

tently, the actin plaques were obviously observed at 72 h, but could not be found at 24 h and only a small number of actin plaques were observed at 48 h (Fig. 5*B*). These results suggest that WDR1 regulating Cofilin phosphorylation is overdosed in cells.

To further examine the regulation of WDR1 on Cofilin phosphorylation, WDR1 was overexpressed in both ES and MEF cells. Cofilin phosphorylation was not obviously different in both WDR1 overexpressed and control cells (Fig. 5, *C* and *D*). When WDR1 was re-expressed in knock-out ES cells, P-Cofilin was obviously increased and comparable with the control (Fig. 5*E*).

WDR1 Regulates Cofilin Phosphorylation via LIMK1—To investigate how WDR1 regulates Cofilin phosphorylation, WDR1 with a FLAG tag was overexpressed in MEF cells and an immunoprecipitation (IP) experiment was performed with FLAG antibody. Our results showed that WDR1 precipitated LIMK1, but not SSH1, PDXP, or TESK1 (Fig. 6*A*). We further docked the binding domains of LIMK1 in 293T cells (Fig. 6*B*). Our results showed that LIMK1-FL and LIMK1–415, but not LIMK1–766, pulled down WDR1 (Fig. 6*B*). We also examined the levels of P-LIMK1 and total LIMK1 in control and *Wdr1* KO MEF cells. Our results showed that both P-LIMK1 and total LIMK1 levels were almost similar in control and KO MEF cells (Fig. 6*C*).

Previous reports showed that LIMK1 activity was inhibited by binding with BMP-RII (bone morphogenetic proteins receptor II) or microtubules (21, 37, 38). Because the LIMK1 antibody did not work well for immunostaining, LIMK1 with the Myc tag was overexpressed in control and *Wdr1* KO MEF cells to examine whether WDR1 regulates LIMK1 by changing its localization. Our results showed that LIMK1 was diffused in both control and KO MEF cells, but was more concentrated to microtubules in *Wdr1* KO MEF cells. We then treated the MEF cells to lightly damage the microtubule structure with a small dosage of nocodazol (1.25 μg/ml), a microtubules depolymerization reagent, and examined P-Cofilin by Western blotting analysis in these cells. Our results showed that P-Cofilin was up-regulated in *Wdr1* KO MEF cells, but was virtually unchanged in the controls (Fig. 6*E*). Our IP experiment showed that WDR1 interacts with the PDZ domain of LIMK1, which is a microtubule binding domain (17). Thus, we concluded that WDR1 might regulate LIMK1 function by inhibiting its binding to microtubules.

Lacking of WDR1 Decreases Cofilin Phosphorylation and Disturbs Actin Structure in Both Mouse Blastocyst Outgrowth and Oocytes—To examine effects of WDR1 loss on F-actin and Cofilin phosphorylation during embryonic development, the blastocysts cultured *in vitro* for 3 days were stained by phalloidin. Actin filaments were orderly and homogeneous in the control (CTL), whereas random actin plaques were observed in *Wdr1*$^{-/-}$ (knock-out, KO) blastocyst outgrowth (Fig. 7*A*). The P-Cofilin level in KO outgrowth was much lower than that in control (Fig. 7*B*). F-actin and P-Cofilin were also examined in mouse GV oocytes by staining and Western blotting analysis. Our results showed that actin was concentrated to some small plaques in the cytoplasm of *Wdr1*$^{-/-}$ (oKO) GV oocytes (Fig. 7*C, arrowheads*), and uniformly distributed in *Wdr1*$^{f/f}$ (CTL) (Fig. 7*C*). P-Cofilin was also dramatically decreased in *Wdr1*$^{-/-}$ GV oocytes compared with the control (Fig. 7*D*).

Discussion

WDR1 and its involvement in actin cytoskeleton play important roles in multiple processes during mouse development (27, 30, 31). However, the role of WDR1 in mouse early embryogen-

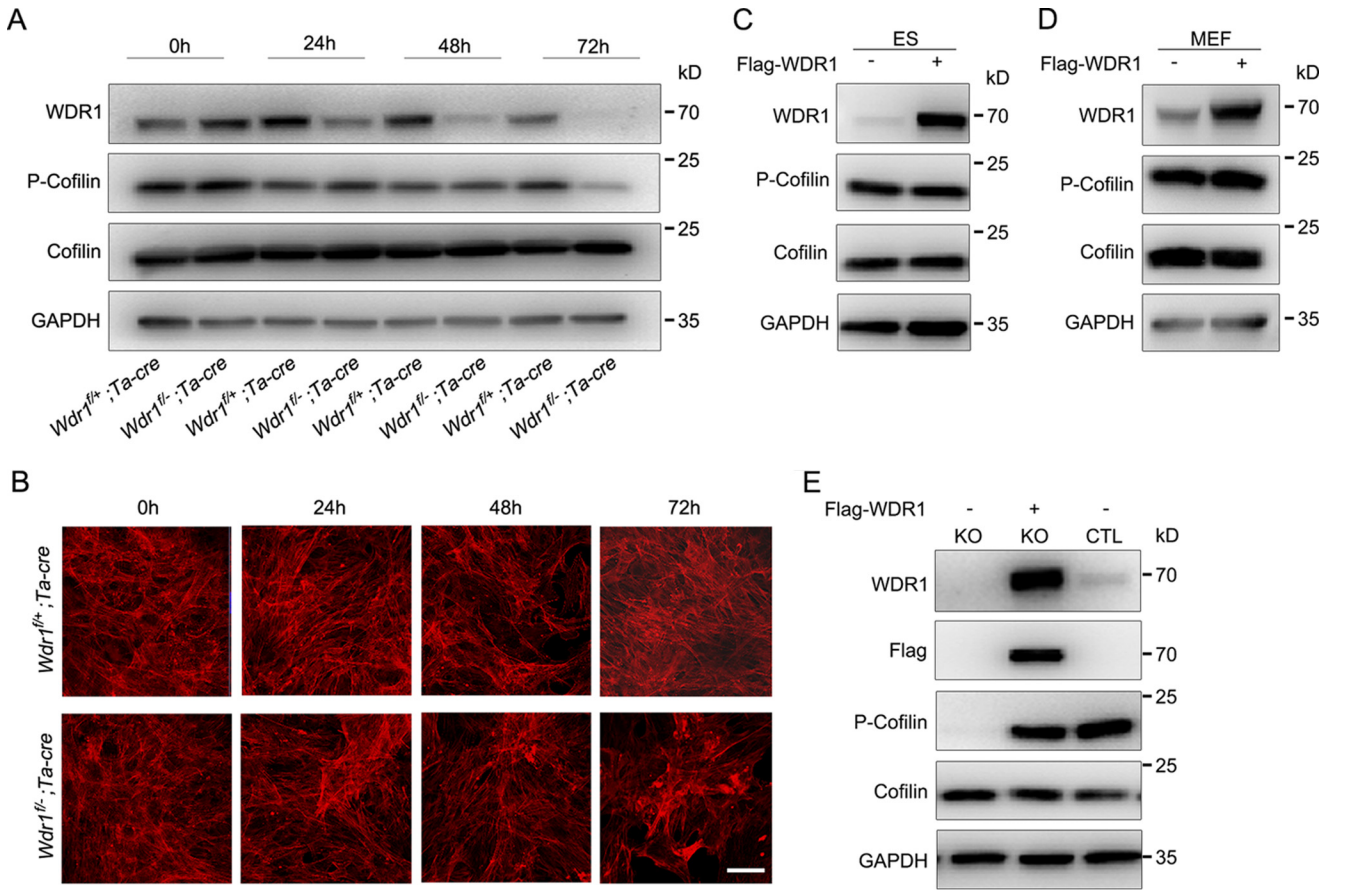

FIGURE 5. **The regulation of WDR1 on Cofilin phosphorylation.** *A*, *Wdr1*$^{+/-}$; *Cre-ER*^{TM} and *Wdr1*$^{f/-}$; *Cre-ER*^{TM} MEF cells were lysed after tamoxifen treatment at 0, 24, 48, and 72 h. Immunoblots of the samples were probed by antibodies to P-Cofilin, Cofilin, WDR1, and GAPDH (loading control). *B*, *Wdr1*$^{+/-}$; *Cre-ER*^{TM} and *Wdr1*$^{f/-}$; *Cre-ER*^{TM} MEF cells were stained with Alexa Fluor® 546 Phalloidin (F-actin, *red*) after tamoxifen treatment for 0, 24, 48, and 72 h. *Scale bar*, 80 μm. *C* and *D*, ES (*C*) and MEF (*D*) cells were infected by adenovirus containing the vector including WDR1 with a FLAG tag. Lysates of control and overexpressed cells were detected by Western blotting with P-Cofilin, Cofilin, WDR1, and GAPDH (loading control) antibodies. *E*, WDR1 was re-expressed in KO ES cells through adenovirus. Cell lysates were detected by antibodies to FLAG, WDR1, P-Cofilin, and Cofilin, GAPDH serving as a loading control.

esis is still largely unknown. In the present study, we showed that depletion of *Wdr1* in oocytes by *Zp3-cre* has no impact on ovulation and pre-implantation embryogenesis, and the oocyte-specific KO females deliver offspring comparable with the controls when they are mated with wild type males. Furthermore, *Wdr1* KO ES cells can be established and have no obvious defects in pluripotency and proliferation. Mouse embryos depleted with zygotic *Wdr1* are lost at a very early stage of development at E5.5, although these embryos can implant and induce decidualization. Consistently, *Wdr1* KO blastocysts can hatch and adhere, but have impaired outgrowth and cannot be labeled with EdU, accompanying the severe defects of actin cytoskeleton. *Wdr1* KO MEF cells have growth defects such as losing S phase and abnormal actin plaques, similar to the phenotypes observed in *Wdr1*-specific KO cardiomyocytes and sertoli cells (30, 31). For successful development, mouse trophoblast cells dramatically differentiate and proliferate, accompanying tremendous changes in cytoskeleton after implantation (39, 40). Although the exact reason that WDR1 loss of function results in the embryonic arrest at E5.5 is unclear, the role of WDR1 in actin cytoskeleton might be critical in the differentiation and growth of trophoblast cells. Thus, the function of WDR1 regulating actin disassembly might be a cell-type specific manner for cell proliferation and survival. Taken together, our results demonstrate that WDR1 plays essential roles in mouse peri-implantation development.

Cofilin is important for spatial and temporal regulation of F-actin dynamics in cells and its activity is tightly controlled by several mechanisms (7, 41, 42). However, which mechanism is the most important process for Cofilin severing activity is still unclear. Cofilin binding and severing F-actin activity is dependent upon its phosphorylation, which is tightly regulated by the protein kinases and phosphatases *in vivo*, such as LIMK and SSH (15, 42). In response to the stimuli, the kinases phosphorylate, whereas the phosphatases dephosphorylate Cofilin to control its interaction with actin for optimal severing activity to regulate the dynamics of actin cytoskeleton (14, 44). In addition, some small molecules or actin-binding protein ligands can competitively displace Cofilin to decrease the binding density of this protein on F-actin into a range that favors severing activity (43, 44). These results suggest that the regulation of Cofilin binding to F-actin is controlled by multiple mechanisms and might be the primary process for Cofilin severing activity *in vivo*.

Most studies have shown that WDR1 significantly accelerated Cofilin dissembling of actin cytoskeleton. However, how WDR1 regulates Cofilin severing activity remains obscure. In the current study, we established *Wdr1* KO ES, MEF cells,

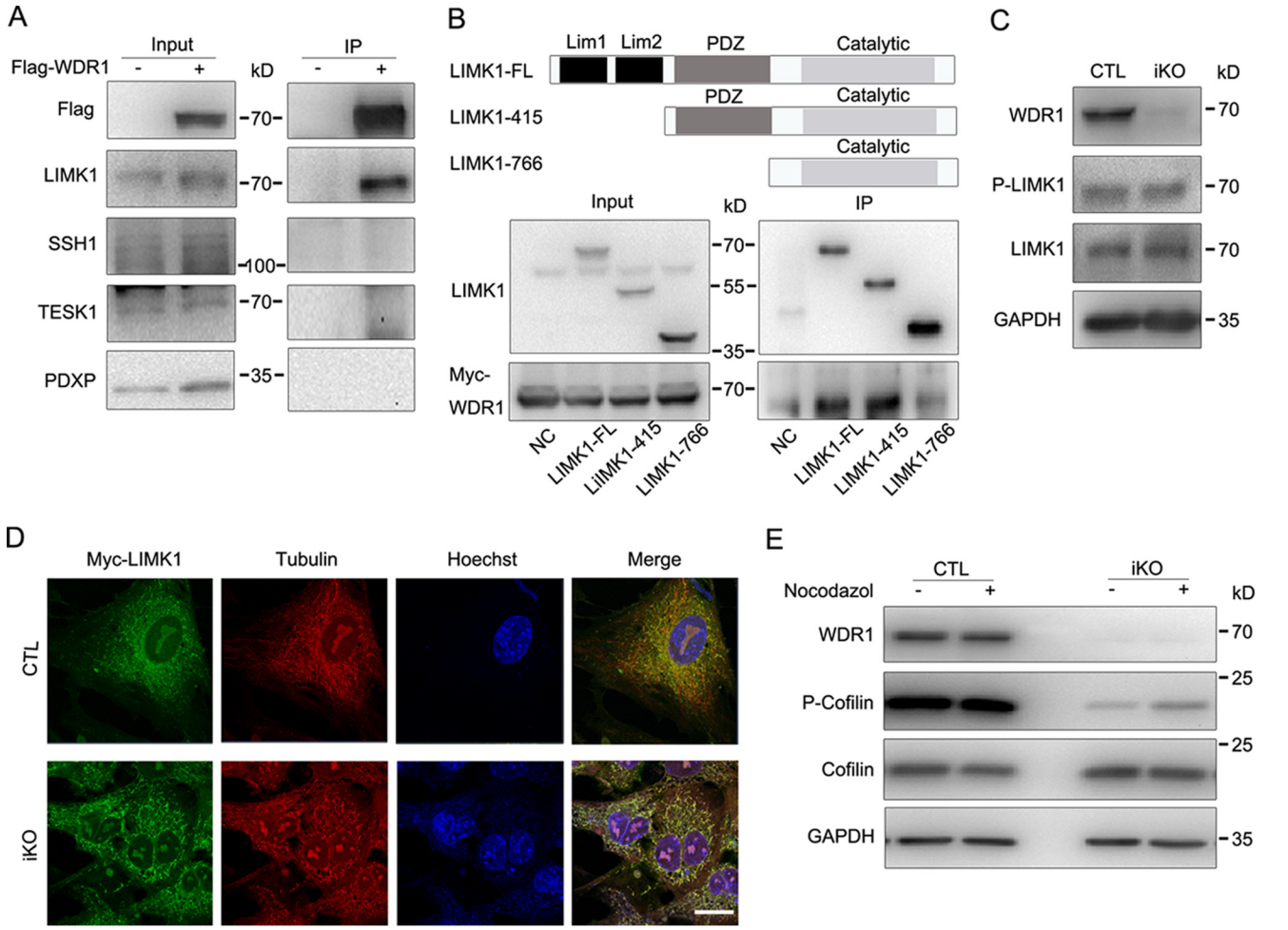

FIGURE 6. **WDR1 regulates Cofilin phosphorylation through LIMK1.** *A*, the control and WDR1 overexpressed MEF cells were immunoprecipitated with anti-FLAG antibody. LIMK1, SSH1, PDXP, and TESK1 were detected by immunoblot in the precipitation products with the specific antibodies. *B*, P-LIMK1 and total-LIMK1 were examined by immunoblot in control and WDR1 knock-out MEF cells. *C*, WDR1 with a Myc tag was co-expressed with LIMK1-FL (full-length), LIMK1–415 (expressed from 415 bases), and LIMK1–766 (expressed from 766 bases) with HA tag, respectively. Lysates were immunoprecipitated with anti-HA antibody. The immunoprecipitated products were analyzed by Western blotting with antibodies to LIMK1 and Myc tag. *D*, LIMK1 with a Myc tag was overexpressed in both CTL and *Wdr1* iKO MEF cells. LIMK1 and microtubules were stained by antibodies to Myc tag (*green*) and α-tubulin (*red*). *Scale bar*, 20 μm. *E*, control and knock-out MEF cells were treated with 1.25 μg/ml of nocodazol for 5 min. Then, P-Cofilin, total-Cofilin, and WDR1 in the cell lysates were detected by immunoblot. GAPDH was used as a loading control.

oocytes, and early embryos to investigate the regulation of WDR1 on Cofilin. Unexpectedly, we found that loss of WDR1 down-regulates P-Cofilin in all examined cells. Consistent with this, a very recent report showed that P-Cofilin is decreased in the cells of some patients with *Wdr1* mutation (45). Interestingly, WDR1 seems to be present in an excessive amount in the cells, which well explains the discrepancies of Cofilin phosphorylation levels observed in knockdown and KO cells (36). We also found that WDR1 interacts with the LIMK1 PDZ region, which was reported to bind to microtubule (17). In addition, LIMK1 is concentrated to the microtubules in *Wdr1* KO MEF cells and the disassembly of microtubules can partly rescue the phosphorylated Cofilin in these cells. Previous reports show that the PDZ domain is a cytoskeleton binding domain and the PDZ domain can localize LIMK1 to the microtubules (21, 37, 38). Thus, these results suggest that WDR1 might inhibit the binding of LIMK1 to microtubules and release LIMK1 to the cytoplasm to catalyze Cofilin phosphorylation, therefore regulating the binding of F-actin to Cofilin.

Previous results show that WDR1 can bind to Cofilin-actin and induces F-actin structural changes to accelerate Cofilin severing F-actin activity (9). In addition, another report shows that WDR1 might simply compete with Cofilin and dissociate redundant Cofilin from F-actin to accelerate severing activity (44). Furthermore, this regulation of Cofilin severing activity is dependent on the pH (46). In our study, we found WDR1 regulated Cofilin phosphorylation through LIMK1 to control the binding of Cofilin with actin filaments. Thus, WDR1 regulates Cofilin severing F-actin activity at multiple layers, suggesting the interrelationship of WDR1 and Cofilin is very complex *in vivo*.

It is worth mentioning that WDR1 depletion decreases the level of Cofilin phosphorylation and disrupts the actin structure in mouse oocytes, but does not affect oocyte maturation and fertilization. Similar observations are also reported in some other cytoskeleton relative proteins in mouse oocytes (47). These results indicate mouse oocytes and very early embryos might have tolerance to some level of actin deficiency. Taking together, our results demonstrate that WDR1 is essential for

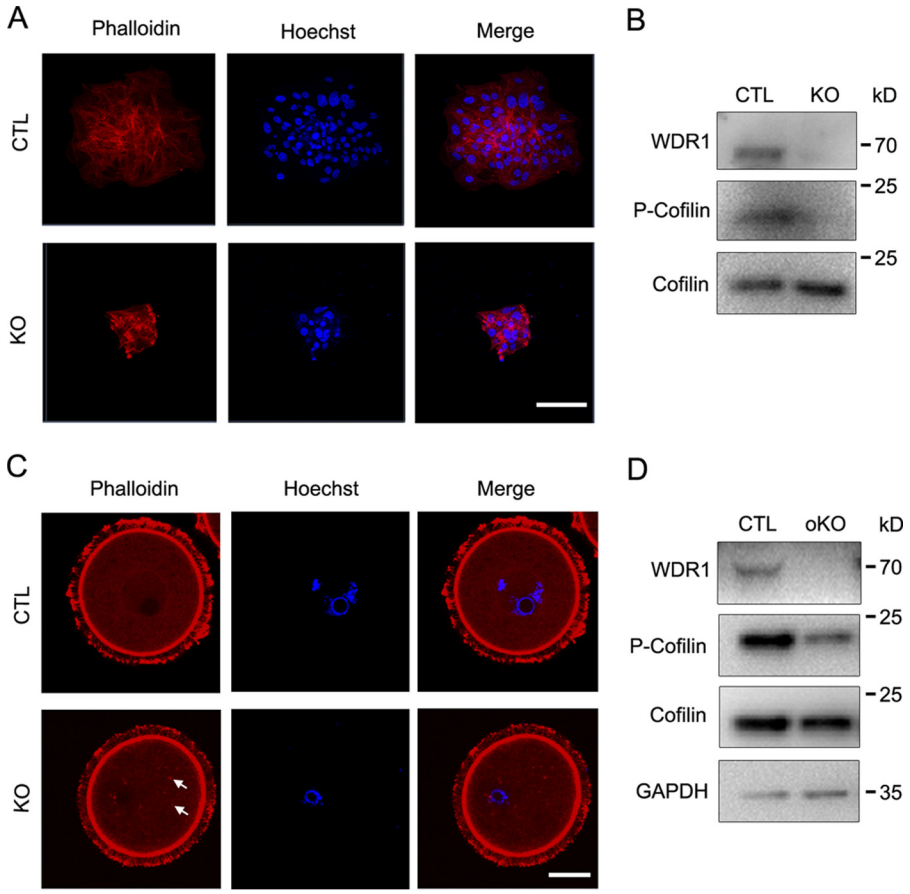

FIGURE 7. **P-Cofilin is down-regulated in *Wdr1* KO blastocyst outgrowth and oocytes.** *A, $Wdr1^{f/-}$ (CTL)* and *$Wdr1^{-/-}$ (KO)* outgrowth of blastocysts were stained after *in vitro* culturing for 3 days by Alexa Fluor® 546 phalloidin (*red*) for actin structure and Hoechst 33342 (*blue*) for DNA. *Scale bar*, 200 μm. *B,* the outgrowths of blastocysts were harvested after culturing for 3 days and subjected to Western blotting with antibodies to WDR1, P-Cofilin, and total-Cofilin. *C, $Wdr1^{f/f}$ (CTL)* and *$Wdr1^{-/-}$ (oKO)* GV oocytes were stained by Alexa Fluor® 546 Phalloidin (F-actin, *red*) and Hoechst 33342 (DNA, *blue*). *Scale bar*, 20 μm. *D,* WDR1, P-Cofilin, and total-Cofilin were detected by Western blotting in 20 GV oocytes from control or WDR1 oocyte-specific KO females, and GAPDH was used as a loading control.

mouse peri-implantation development and regulates Cofilin phosphorylation through LIMK1 to optimize its F-actin severing activity *in vivo*.

Experimental Procedures

Mice Maintenance—In compliance with the guidelines of the Animal Care and Use Committee of the Institute of Zoology at the Chinese Academy of Sciences, the *$Wdr1^{f/f}$*; *Zp3-cre* and *$Wdr1^{f/f}$*; *Cre-ER^{TM}* mouse lines were maintained on a mixed background (129/C57BL/6). A pair of Flox sequences was inserted in both ends of the fourth exon of *Wdr1* to establish *$Wdr1^{f/f}$* mice as previously described (31). *Zp3-cre* mice (48) were mated with *$Wdr1^{f/f}$* mice to obtain the oocyte-specific *Wdr1* knock-out females. To establish *Wdr1* inducible knock-out MEF cell lines, *$Wdr1^{f/-}$* mice were mated with *Cre-ER^{TM}* transgenic mice (49) to obtain *$Wdr1^{+/-}$*; *Cre-ER^{TM}* offspring. E13.5 fetuses from the mating of *$Wdr1^{+/-}$*; *Cre-ER^{TM}* females with *$Wdr1^{f-}$* males were used to derive the MEF cells. All mice were maintained in SPF animal houses with a 12-h light/12-h dark cycle. Mouse tail tip or cells were lysed by an alkaline lysate buffer at 95 °C for 1 h. Then genotyping PCR was conducted with specific primers (Table 1).

Collection and Culture of Mouse Eggs and Embryos—GV oocytes were collected using M199 medium from ovaries. After female mice were stimulated by injecting PMSG and hCG (Ningbo Second Hormone Factory), metaphase II (MII) oocytes were collected in M2 medium from oviducts after hCG 13 h; 1-cell, 2-cell embryos, and morulas were flushed from oviducts at E0.5, E1.5, and E2.5 days; and blastocysts were collected from uteruses at E3.5. Blastocysts were cultured in 1066 medium supplemented with 10% FBS, 1 μM sodium pyruvate, 2 μM L-glutamine, and 50 μg/ml of penicillin/streptomycin at 37 °C in 5% CO_2 (50, 51). The culture dishes for blastocysts were pre-treated with 0.2% gelatin. For the E5.5 embryos section, the deciduas were frozen at −80 °C.

Cell Culturing—*Wdr1* inducible knock-out MEF cell lines were derived from *$Wdr1^{F/-}$*; *Cre-ER^{TM}* fetuses at E13.5 and *$Wdr1^{+/-}$*; *Cre-ER^{TM}* fetuses as the control. Tamoxifen was added to the medium to induce the *Wdr1* knock-out. The 293T cell line was cultured in DMEM with 10% FBS.

Wdr1 knock-out ES cell lines were established from *$Wdr1^{-/-}$* blastocysts as in a previous report (52), *$Wdr1^{f/-}$* ES cells were used as control. Briefly, blastocysts were cultured in 0.2% gelatin-pretreated dishes in N2B27 medium supplemented with PD0325901 (1 μM, catalogue number P-9688, LC Laboratories), CHIR99021 (3 μM, catalogue number C-6556, LC Laboratories), and LIF (1000 units/ml, catalogue number

TABLE 1
Primers for genotyping, qRT-PCR and plasmid construction

Gene		Sequence (5′-3′)
Genotyping		
Wdr1-Flox	Forward	GCTATAAATGAGGTCCTGATGAG
	Reverse	TCAGGCTTACAAAGCTCACATG
Wdr1-deletion	Forward	GCTATAAATGAGGTCCTGATGAG
	Reverse	TTGCACAGAGGTGAATGACAGAG
Zp3-cre	Forward	CAGATGAGGTTTGAGGCCACAG
	Reverse	TTCTTGCGAACCTCATCACTC
Global cre	Forward	TCCAATTTACTGACCGTACACCAA
	Reverse	CCTGATCCTGGC AATTTCGGCTA
qRT-PCR		
Wdr1	Forward	TGAGTACCAGCCTTTCGCTG
	Reverse	AGACAGCTCCAAACTTCTCCC
Pax6	Forward	TAACGGAGAAGACTCGGATGAAGC
	Reverse	CGGGCAAACACATCTGGATAATGG
T	Forward	CCTCCATGTGCTGAGACTTG
	Reverse	TCACAAAAAACTGGACCACA
Sox17	Forward	TAAATGCCTTGAGGGACTTG
	Reverse	GTTTCTTAGATGCATTTTCTTACC
Gapdh	Forward	CCCCAATGTGTCCGTCGTG
	Reverse	TGCCTGCTTCACCACCTTCT
Plasmid construction		
Flag-Wdr1	Forward	ATGCTCTAGAGCCACCATGGATTACAAGGATGACGACGATAAGATGC
	Reverse	CCCTCAGTAGGTGATTGT
Wdr1	Forward	CAAGTCTCGAGGGATGCCGTACGAGATCAAGAAG
	Reverse	TGAGGCGGCCGCTCAGTAGGTGATTGT
Limk1-FL	Forward	TTCGGTCGACATGAGGTTGACGCTACTT
Limk1–415	Forward	GGAAGATCTCTCCTCGTGTCTATCCCAGC
Limk1–766	Forward	GCCCGAATTCGGCACGACCCCCATGACTC
	Reverse	ATCGGCGGCCGCTCAGTCAGGGGTGGGCAGGCA

ESG1107, Millipore) (2i/LIF medium) for 5 days. Then, the inner cell mass clones were digested by trypsin substitution and planted onto MEF cell feeders in 2i/LIF medium or DMEM containing 15% fetal bovine serum, 2 mM sodium pyruvate, 2 mM L-glutamine, 0.1 mM nonessential amino acids, 50 μg/ml of penicillin/streptomycin, 0.1 mM β-mercaptoethanol, and 10 ng/ml of LIF (ES serum medium). For cell number counting, ES cells cultured on gelatin were digested to single cells and counted in a blood counting chamber. All cell lines were cultured at 37 °C in 5% CO_2.

ES Cell Differentiation—ES cells were labeled with EGFP, digested to single cells, resuspended in DMEM with 15% FBS, and kept on ice. Blastocysts were collected from the uterus of E3.5 superovulated ICR females. 10–15 ES cells were picked up and injected into one blastocyst cavity by an injection pipette. The injected blastocysts were cultured in gelatin-pretreated dishes for 3 days. ES cells in the chimeras were detected by fluorescence confocal microscopy. For EB formation, ES cells were digested to single cells and cultured by seeding 600 cells in one 30-μl hanging droplet of ES serum medium without LIF.

Real-time RT-PCR—Total RNA was extracted from cells with the RNAzol® RT RNA Isolation Reagent (Molecular Research Center) and isolated from oocytes and pre-implantation embryos with the Dynabeads mRNA Direct Micro Kit (Ambion). The RNA was then reversely transcripted with the PrimeScript™ RT-PCR kit (Takara). The primer sequences were listed in Table 1. Real-time PCR was carried out in the All-In-One RT Master Mix G490 system (Applied Biological Materials). GAPDH was used as a reference gene for normalization of the mRNA levels. Data were processed using the $2^{-\Delta\Delta Ct}$ method.

Plasmid Construction and Lentivirus Transfection—293FT cells were transfected with the envelope plasmid pMD2G, packaging plasmid psPAX2, and core expression plasmid pHIV-EGFP (Addgene) by PEI. After culturing for 48 and 72 h, the lentivirus supernatant was collected and concentrated through ultracentrifugation at 17,000 rpm for 2 h. For transfection, MEF or ES cells were incubated with lentivirus for 12 h and then cultured with regular medium. For protein expression in 293FT cells, genes were linked to HA-pCMV or Myc-pCMV vector. *Wdr1* was added at the FLAG sequence in the forward primer, and linked to pHIV-EGFP through XbaI and SmaI sites. Full-length *Limk1*, *Limk1*-415 (deleted two Lim domains), and *Limk1*-766 (deleted two Lim domains and PDZ domain) were added by the respective forward primer and a common reverse primer, and then linked to pCMV-HA vector through forward sites SalI, BglII, and EcoRI and reverse site NotI. *Wdr1* was linked to pCMV-Myc vector through XhoI and NotI sites. The primer sequences for vector construction are listed in Table 1.

Immunoblots and Immunoprecipitation—Samples for IP were lysed by IP/Western lysis buffer (Byotime) with protease inhibitor mixture (Roche Applied Science) and 5 mM NaF. For IP, 5% of the lysates served as input and the rest were incubated with mouse anti-FLAG antibody (1:500, Abmart) or mouse anti-HA antibody (1:500, Abmart) and protein G-agarose (Santa Cruz) at 4 °C for 5 h. These samples were diluted with a SDS loading buffer, heated at 95 °C for protein denaturalization, and then analyzed by Western blotting. Oocytes, embryos, and cells samples for Western blotting were also lysed and denaturalized by the same buffers.

Samples for immunoblots were separated by 10% SDS-PAGE and transferred to PVDF membranes (Invitrogen). The PVDF membranes were blocked with 5% skim milk and incubated with the primary antibody at 4 °C overnight. After being washed three times with PBS supplemented with 0.1% Tween 20, the PVDF membranes were incubated with HRP-conju-

gated secondary antibodies. The signals were developed by SuperSignal West Dura Extended Duration Substrate (Pierce).

Primary antibodies included: rabbit anti-WDR1 (1:1,000, catalogue number 13676-1-AP, Proteintech), rabbit anti-phospho-Cofilin (Ser-3, 1:1,000, catalogue number 3313, Cell Signaling Technology), rabbit anti-Cofilin (1:1,000, catalogue number 5175, Cell Signaling Technology), rabbit anti-LIMK1 (1:1,000, catalogue number 3842, Cell Signaling Technology), rabbit anti-phospho-LIMK1 (1:1,000, catalogue number 3841, Cell Signaling Technology), rabbit anti-PDXP (1:1,000, catalogue number 4686, Cell Signaling Technology), rabbit anti-TESK1 (1:1,000, catalogue number 4655, Cell Signaling Technology), rabbit anti-SSH1 (1:1,000, catalogue 13578, Cell Signaling Technology), rabbit anti-NANOG (1:1,000, catalogue number ab80892, Abcam), mouse anti-SOX2 (1:1,000, catalogue number 3579, Cell Signaling Technology), goat anti-OCT4 (1:1,000, catalogue number sc-8629, Santa Cruz Biotechnology), mouse monoclonal anti-GAPDH (1:5,000, catalogue number 30201ES20, Yeason), mouse monoclonal anti-pan-actin (1:2,000, catalogue number ab75373, Abcam), mouse anti-Myc (1:2,000 catalogue number M20002, Abmart), mouse anti-FLAG (1:1,000 for Western 1:500 for IP, catalogue number M20018, Abmart), and mouse anti-HA (1:500 for IP, catalogue number M20003, Abmart). The second antibodies included: goat anti-rabbit, goat anti-mouse, and rabbit anti-goat, which were conjugated with HRP (1:4,500, Abmart).

G-actin and F-actin Separation—G-actin and F-actin were separated by a two-step extract and ultracentrifugation protocol. The samples from the separated G-actin and F-actin fractions were proportionally loaded and analyzed by Western blotting using an antibody to pan-actin. G-actin was extracted by a cold lysis buffer 1 (10 mM K_2HPO_4, 100 mM NaF, 50 mM KCl, 2 mM $MgCl_2$, 1 mM EGTA, 0.2 mM DTT, 0.5% Triton X-100, 1 mM sucrose, pH 7.0) and centrifuged at 15,000 × *g* for 30 min. Soluble actin (G-actin) was measured in the supernatant. F-actin in the pellet was resuspended in lysis buffer plus an equal volume of buffer 2 (1.5 mM guanidine hydrochloride, 1 mM sodium acetate, 1 mM $CaCl_2$, 1 mM ATP, and 20 mM Tris-HCl, pH 7.5) and incubated on ice for 1 h to convert F-actin into soluble G-actin, with gentle mixing every 15 min. The samples were centrifuged at 15,000 × *g* for 30 min, and F-actin was measured in this supernatant (35).

EdU and PI Staining—Embryos were incubated with 500 μM EdU for 2 h and then fixed with 4% paraformaldehyde. Detection of incorporated EdU was performed using the Cell-Light EdU Apollo 567 *In Vitro* Imaging Kit (RiboBio) according to the manufacturer's protocol.

For cell cycle detecting, MEF cells were digested to single cells and fixed by 70% ethanol at −20 °C overnight. Cells were permeabilized in PBS containing 0.5% Triton X-100 at room temperature for 30 min and then stained by propidium iodide (PI) in PBS at 4 °C for 30 min. PI signals were detected by flow cytometry and the results were analyzed by Flowjo software (Tree Star).

Immunohistochemistry—Cells or blastocysts were fixed by 4% paraformaldehyde in PBS at room temperature for 10 min and permeabilized in PBS containing 0.5% Triton X-100. Cells and embryos were blocked by 5% normal donkey serum at room temperature for 1 h and then incubated in primary antibodies at 4 °C overnight. After being washed with PBS three times to remove unconjugated primary antibodies, second antibodies, Hoechst 33342 (Invitrogen) and Alexa Fluor 546-labeled phalloidin (Invitrogen), were added and incubated at room temperature for 1 h. For Myc-Limk1 staining, MEF cells were fixed by 0.1% glutaraldehyde, 0.1 μM sodium cacodylate, pH 7.3. For GV oocyte F-actin staining, oocytes were fixed with 130 mM KCl, 25 mM HEPES, pH 7.0, 3 mM $MgCl_2$, 4% paraformaldehyde, 0.15% glutaraldehyde, and 0.06% Triton X-100 at room temperature for 2 h and permeabilization was extended to 30 min.

Primary antibodies included: rabbit anti-Cofilin (1:100), rabbit anti-Myc (1:100, catalogue number 2278, Cell Signaling Technology), and mouse anti-α-tubulin (1:200, catalogue number F2168, Sigma). The secondary antibodies included: donkey anti-mouse conjugated with Alexa Fluor 549 (1:200), donkey anti-rabbit conjugated with Alexa Fluor 488 (1:500), and donkey anti-rabbit conjugated with Alexa Fluor 633 (1:500) (Invitrogen, Life Technologies). Immunofluorescent images were obtained on an Axioplan Zeiss microscope (LSM780, Carl Zeiss, Thornwood, NY) and the intensity of the immunofluorescent signal was analyzed with ZEN lite 2011 (Carl Zeiss).

Statistical Analyses—Quantitative analyses were carried out with GraphPad Prism software with at least 3 independent biological samples and expressed as the mean ± S.D. *p* values of comparisons between 2 groups were calculated using Student's *t* test. $p < 0.05$ was considered as significant.

Author Contributions—Y. X. designed and performed major experiments, analyzed the data, and wrote the manuscript. H. M. conducted Limk1 overexpression experiments. W. P. established the $Wdr1^{f/f}$ mouse line. D. Q. harvested GV oocytes and stained F-actin structure. X. W., Z. X., Y-L. X., and W. L. established MEF cell lines, injected ES cells into blastocysts, and performed H&E staining of embryo sections. L. L., Y. Z., and C. J. initiated and organized this project, analyzed the data, and wrote the manuscript. All authors commented on the manuscript.

References

1. Schejter, E. D., and Wieschaus, E. (1993) Functional elements of the cytoskeleton in the early *Drosophila* embryo. *Annu. Rev. Cell Biol.* **9,** 67–99
2. Heller, E., and Fuchs, E. (2015) Tissue patterning and cellular mechanics. *J. Cell Biol.* **211,** 219–231
3. Yae, K., Keng, V. W., Koike, M., Yusa, K., Kouno, M., Uno, Y., Kondoh, G., Gotow, T., Uchiyama, Y., Horie, K., and Takeda, J. (2006) Sleeping beauty transposon-based phenotypic analysis of mice: lack of Arpc3 results in defective trophoblast outgrowth. *Mol. Cell. Biol.* **26,** 6185–6196
4. Brieher, W. (2013) Mechanisms of actin disassembly. *Mol. Biol. Cell* **24,** 2299–2302
5. Bugyi, B., and Carlier, M. F. (2010) Control of actin filament treadmilling in cell motility. *Annu. Rev. Biophys.* **39,** 449–470
6. Pollard, T. D. (2016) Actin and actin-binding proteins. *Cold Spring Harbor Perspect. Biol.* **8,** pii: a018226
7. Bernstein, B. W., and Bamburg, J. R. (2010) ADF/cofilin: a functional node in cell biology. *Trends Cell Biol.* **20,** 187–195
8. Andrianantoandro, E., and Pollard, T. D. (2006) Mechanism of actin filament turnover by severing and nucleation at different concentrations of ADF/cofilin. *Mol. Cell* **24,** 13–23
9. Gressin, L., Guillotin, A., Guérin, C., Blanchoin, L., and Michelot, A. (2015) Architecture dependence of actin filament network disassembly. *Curr. Biol.* **25,** 1437–1447
10. Ohashi, K. (2015) Roles of cofilin in development and its mechanisms of regulation. *Dev. Growth Differ.* **57,** 275–290

11. Bamburg, J. R., and Wiggan, O. P. (2002) ADF/cofilin and actin dynamics in disease. *Trends Cell Biol.* **12,** 598–605
12. Bamburg, J. R., Bernstein, B. W., Davis, R. C., Flynn, K. C., Goldsbury, C., Jensen, J. R., Maloney, M. T., Marsden, I. T., Minamide, L. S., Pak, C. W., Shaw, A. E., Whiteman, I., and Wiggan, O. (2010) ADF/Cofilin-actin rods in neurodegenerative diseases. *Curr. Alzheimer Res.* **7,** 241–250
13. Nishida, E., Maekawa, S., and Sakai, H. (1984) Cofilin, a protein in porcine brain that binds to actin filaments and inhibits their interactions with myosin and tropomyosin. *Biochemistry* **23,** 5307–5313
14. Kaji, N., Muramoto, A., and Mizuno, K. (2008) LIM kinase-mediated cofilin phosphorylation during mitosis is required for precise spindle positioning. *J. Biol. Chem.* **283,** 4983–4992
15. Mizuno, K. (2013) Signaling mechanisms and functional roles of cofilin phosphorylation and dephosphorylation. *Cell Signal.* **25,** 457–469
16. Arber, S., Barbayannis, F. A., Hanser, H., Schneider, C., Stanyon, C. A., Bernard, O., and Caroni, P. (1998) Regulation of actin dynamics through phosphorylation of cofilin by LIM-kinase. *Nature* **393,** 805–809
17. Edwards, D. C., and Gill, G. N. (1999) Structural features of LIM kinase that control effects on the actin cytoskeleton. *J. Biol. Chem.* **274,** 11352–11361
18. Niwa, R., Nagata-Ohashi, K., Takeichi, M., Mizuno, K., and Uemura, T. (2002) Control of actin reorganization by Slingshot, a family of phosphatases that dephosphorylate ADF/cofilin. *Cell* **108,** 233–246
19. Toshima, J., Toshima, J. Y., Amano, T., Yang, N., Narumiya, S., and Mizuno, K. (2001) Cofilin phosphorylation by protein kinase testicular protein kinase 1 and its role in integrin-mediated actin reorganization and focal adhesion formation. *Mol. Biol. Cell* **12,** 1131–1145
20. Gohla, A., Birkenfeld, J., and Bokoch, G. M. (2005) Chronophin, a novel HAD-type serine protein phosphatase, regulates cofilin-dependent actin dynamics. *Nat. Cell Biol.* **7,** 21–29
21. Foletta, V. C., Lim, M. A., Soosairajah, J., Kelly, A. P., Stanley, E. G., Shannon, M., He, W., Das, S., Massague, J., Bernard, O., and Soosairaiah, J. (2003) Direct signaling by the BMP type II receptor via the cytoskeletal regulator LIMK1. *J. Cell Biol.* **162,** 1089–1098
22. Döppler, H., Bastea, L. I., Eiseler, T., and Storz, P. (2013) Neuregulin mediates F-actin-driven cell migration through inhibition of protein kinase D1 via Rac1 protein. *J. Biol. Chem.* **288,** 455–465
23. Oleinik, N. V., Helke, K. L., Kistner-Griffin, E., Krupenko, N. I., and Krupenko, S. A. (2014) Rho GTPases RhoA and Rac1 mediate effects of dietary folate on metastatic potential of A549 cancer cells through the control of cofilin phosphorylation. *J. Biol. Chem.* **289,** 26383–26394
24. Cooper, J. A., and Schafer, D. A. (2000) Control of actin assembly and disassembly at filament ends. *Curr. Opin. Cell Biol.* **12,** 97–103
25. Brieher, W. M., Kueh, H. Y., Ballif, B. A., and Mitchison, T. J. (2006) Rapid actin monomer-insensitive depolymerization of Listeria actin comet tails by cofilin, coronin, and Aip1. *J. Cell Biol.* **175,** 315–324
26. Rodal, A. A., Tetreault, J. W., Lappalainen, P., Drubin, D. G., and Amberg, D. C. (1999) Aip1p interacts with cofilin to disassemble actin filaments. *J. Cell Biol.* **145,** 1251–1264
27. Kile, B. T., Panopoulos, A. D., Stirzaker, R. A., Hacking, D. F., Tahtamouni, L. H., Willson, T. A., Mielke, L. A., Henley, K. J., Zhang, J. G., Wicks, I. P., Stevenson, W. S., Nurden, P., Watowich, S. S., and Justice, M. J. (2007) Mutations in the cofilin partner Aip1/Wdr1 cause autoinflammatory disease and macrothrombocytopenia. *Blood* **110,** 2371–2380
28. Ren, N., Charlton, J., and Adler, P. N. (2007) The flare gene, which encodes the AIP1 protein of *Drosophila*, functions to regulate F-actin disassembly in pupal epidermal cells. *Genetics* **176,** 2223–2234
29. Gerisch, G., Faix, J., Köhler, J., and Müller-Taubenberger, A. (2004) Actin-binding proteins required for reliable chromosome segregation in mitosis. *Cell Motil. Cytoskeleton* **57,** 18–25
30. Xu, J., Wan, P., Wang, M., Zhang, J., Gao, X., Hu, B., Han, J., Chen, L., Sun, K., Wu, J., Wu, X., Huang, X., and Chen, J. (2015) AIP1-mediated actin disassembly is required for postnatal germ cell migration and spermatogonial stem cell niche establishment. *Cell Death Dis.* **6,** e1818
31. Yuan, B., Wan, P., Chu, D., Nie, J., Cao, Y., Luo, W., Lu, S., Chen, J., and Yang, Z. (2014) A cardiomyocyte-specific Wdr1 knockout demonstrates essential functional roles for actin disassembly during myocardial growth and maintenance in mice. *Am. J. Pathol.* **184,** 1967–1980
32. Liu, L. J., Zhang, X. Y., He, N., Liu, K., Shi, X. G., Feng, T., Geng, T. T., Yuan, D. Y., Kang, L. L., and Jin, T. B. (2016) Genetic variation in WDR1 is associated with gout risk and gout-related metabolic indices in the Han Chinese population. *Genet. Mol. Res.* **15,** 10.4238/gmr.15027381
33. Qi, D., Wu, B., Tong, D., Pan, Y., and Chen, W. (2015) Identification of key transcription factors in caerulein-induced pancreatitis through expression profiling data. *Mol. Med. Rep.* **12,** 2570–2576
34. Xu, H., Chen, Y., Tan, C., Xu, T., Yan, Y., Qin, R., Huang, Q., Lu, C., Liang, C., Lu, Y., Wang, H., and Chen, J. (2016) High expression of WDR1 in primary glioblastoma is associated with poor prognosis. *Am. J. Transl. Res.* **8,** 1253–1264
35. Huang, W., Zhu, P. J., Zhang, S., Zhou, H., Stoica, L., Galiano, M., Krnjević, K., Roman, G., and Costa-Mattioli, M. (2013) mTORC2 controls actin polymerization required for consolidation of long-term memory. *Nat. Neurosci.* **16,** 441–448
36. Luxenburg, C., Heller, E., Pasolli, H. A., Chai, S., Nikolova, M., Stokes, N., and Fuchs, E. (2015) Wdr1-mediated cell shape dynamics and cortical tension are essential for epidermal planar cell polarity. *Nat. Cell Biol.* **17,** 592–604
37. Lee-Hoeflich, S. T., Causing, C. G., Podkowa, M., Zhao, X., Wrana, J. L., and Attisano, L. (2004) Activation of LIMK1 by binding to the BMP receptor, BMPRII, regulates BMP-dependent dendritogenesis. *EMBO J.* **23,** 4792–4801
38. Gorovoy, M., Niu, J., Bernard, O., Profirovic, J., Minshall, R., Neamu, R., and Voyno-Yasenetskaya, T. (2005) LIM kinase 1 coordinates microtubule stability and actin polymerization in human endothelial cells. *J. Biol. Chem.* **280,** 26533–26542
39. Parast, M. M., Aeder, S., and Sutherland, A. E. (2001) Trophoblast giant-cell differentiation involves changes in cytoskeleton and cell motility. *Dev. Biol.* **230,** 43–60
40. Wang, H., and Dey, S. K. (2006) Roadmap to embryo implantation: clues from mouse models. *Nat. Rev. Genet.* **7,** 185–199
41. Bamburg, J. R. (1999) Proteins of the ADF/cofilin family: essential regulators of actin dynamics. *Annu. Rev. Cell Dev. Biol.* **15,** 185–230
42. Van Troys, M., Huyck, L., Leyman, S., Dhaese, S., Vandekerkhove, J., and Ampe, C. (2008) Ins and outs of ADF/cofilin activity and regulation. *Eur. J. Cell Biol.* **87,** 649–667
43. Elam, W. A., Kang, H., and De La Cruz, E. M. (2013) Competitive displacement of cofilin can promote actin filament severing. *Biochem. Biophys. Res. Commun.* **438,** 728–731
44. Chen, Q., Courtemanche, N., and Pollard, T. D. (2015) Aip1 promotes actin filament severing by cofilin and regulates constriction of the cytokinetic contractile ring. *J. Biol. Chem.* **290,** 2289–2300
45. Kuhns, D. B., Fink, D. L., Choi, U., Sweeney, C., Lau, K., Priel, D. L., Riva, D., Mendez, L., Uzel, G., Freeman, A. F., Olivier, K. N., Anderson, V. L., Currens, R., Mackley, V., Kang, A., *et al.* (2016) Cytoskeletal abnormalities and neutrophil dysfunction in WDR1 deficiency. *Blood* **128,** 2135–2143
46. Nomura, K., Hayakawa, K., Tatsumi, H., and Ono, S. (2016) Actin-interacting protein 1 promotes disassembly of actin-depolymerizing factor/cofilin-bound actin filaments in a pH-dependent manner. *J. Biol. Chem.* **291,** 5146–5156
47. Liang, Q. X., Zhang, Q. H., Qi, S. T., Wang, Z. W., Hu, M. W., Ma, X. S., Zhu, M. S., Schatten, H., Wang, Z. B., and Sun, Q. Y. (2015) Deletion of Mylk1 in oocytes causes delayed morula-to-blastocyst transition and reduced fertility without affecting folliculogenesis and oocyte maturation in mice. *Biol. Reprod.* **92,** 97
48. Lewandoski, M., Wassarman, K. M., and Martin, G. R. (1997) Zp3-cre, a transgenic mouse line for the activation or inactivation of loxP-flanked target genes specifically in the female germ line. *Curr. Biol.* **7,** 148–151
49. Hayashi, S., and McMahon, A. P. (2002) Efficient recombination in diverse tissues by a tamoxifen-inducible form of Cre: a tool for temporally regulated gene activation/inactivation in the mouse. *Dev. Biol.* **244,** 305–318
50. Bedzhov, I., Leung, C. Y., Bialecka, M., and Zernicka-Goetz, M. (2014) *In vitro* culture of mouse blastocysts beyond the implantation stages. *Nat. Protoc.* **9,** 2732–2739
51. Hsu, Y. C. (1971) Post-blastocyst differentiation *in vitro*. *Nature* **231,** 100–102
52. Zhao, Z. A., Yu, Y., Ma, H. X., Wang, X. X., Lu, X., Zhai, Y., Zhang, X., Wang, H., and Li, L. (2015) The roles of ERAS during cell lineage specification of mouse early embryonic development. *Open Biol.* **5,** 10.1098/rsob.150092